morphology and joint kinematics. This system was successfully employed for motion analysis of the cervical spine[12,13] and wrist joint[14,15] and for ascertaining the pathological characteristics of clubfoot.[16] The purpose of this study was to analyze the pattern of RA hindfoot valgus deformity using this method.

MATERIALS AND METHODS

Fourteen patients with RA hindfoot valgus deformity were enrolled from the outpatient orthopedic department of Osaka University Afflicted Hospital. All patients met the American College of Rheumatology criteria (1995) for diagnosis of RA and Vahvanen's standard of valgus deformity (stages I–IV) in clinical manifestation and radiographic films.[6] X-ray films showed no distal tibofibular joint involvement. The mean age was 57 years (range, 39–71 years). The mean duration of disease was 11.7 years (range, 1–32 years). Eight healthy volunteers with no foot pain or medical history of foot disorders were recruited as controls. Their mean age was 27.8 years (range, 24–32 years). All participants gave written informed consent before the study began.

Analysis of RA hindfoot deformity was performed noninvasively, including data acquisition, segmentation, and 3D model reconstruction, and description of the deformity. Finally, the accuracy of this method was validated.

Data Acquisition

Computed tomography was performed on 21 feet of 14 patients with RA, and MRI was performed on 10 normal feet of 8 healthy volunteers who were considered as the control group. In a preliminary test, we found a significant loss of surface information from MRI data for feet from RA patients because of severe inflammation and bone erosion. The loss of surface information distorted the shape of the surface model and led to inaccurate analysis of the deformity pattern. As a sufficient number of RA patients who needed CT scans for preoperative planning were available in the outpatient orthopedic department, the 3D CT data were obtained for the patients with RA. To reduce radiation exposure, data were collected from healthy volunteers who underwent MRI.

CT from the distal third of the tibia and fibula to the end of the foot was performed for each patient using a clinical helical scanner (Light Speed Ultra 16; General Electric Company, Maukesha, WI) that produced 256 consecutive images with a section thickness of 0.625 mm. Scanning parameters were 120 kV and 120 to 240 mA. Total exposure time was about 24 min. MR images were taken using a 1.0 Tesla scanner (Sigma Horizontal LX ver. 9.1; General Electric Company, Milwaukee, WI). A TORSOPA coil was employed, and the 3D image was obtained using a 3D fast-GRASS (gradient recalled acquisition in the steady state) pulse sequence with a TR/TE ratio of recommended/minimum full and 1.5-mm slice thickness. The flip angle was 25°, and a 250-mm field of view (imaging matrix, 256 × 256) was used. Acquisition of each 3D volume imaging took about 3 min.

A custom nonmetallic orthosis was used to immobilize the ankle in a neutral position and to standardize the orientation of the foot relative to the ankle in the scanner. The device held the lower leg on a horizontal cushion and the foot against a vertical plate. With the lower leg secured, the foot position was adjusted until the neutral position of the ankle was achieved, then the foot was secured appropriately. If a neutral position could not be achieved due to an ankle deformity, the foot stayed in its natural unloaded position.

Segmentation and 3D Model Reconstruction

The contour of each hindfoot bone was semi-automatically extracted from 3D images by an intensity threshold technique using Virtual Place M.® software (AZE Ltd., Tokyo) developed in our laboratory. Surface models of the hindfoot and ankle joint of each participant were reconstructed from 3D image data using the marching cubes algorithm, in which areas with the same voxel values were surrounded by triangular patches.[17] Visualization was obtained by applying a modified version of Visualization Toolkit software (Kitware Inc., New York, NY). All left hindfoot 3D models were inverted for comparison with right hindfoot models.

Description of the Deformity

The tibia was used to set up a reference coordinate system, which was considered as the standard coordinate system (SCS). The purpose of using the SCS was to discern the displacements in the ankle, subtalar, and midtarsal joints relative to the tibia in RA patients. Displacement was defined as the change of a bone position from a normal position to a RA deformed position. The SCS was established from modification of the anatomical coordinate system of the tibia proposed by Cappozzo and colleagues.[18] The origin was located at the midpoint of the line joining the lateral malleoli (LM) and the medial malleoli (MM). The y-axis started from the origin and ran upward parallel to the long axis of the tibia. Thus, the y-axis and the line between the LM and MM formed a quasi-frontal plane. The x-axis was perpendicular to the plane defined by the y-axis and the line between the LM and MM, in the forward direction; the z-axis was orthogonal to the x- and y- axes in the lateral direction (Fig. 1). The long axis of the tibia was determined by the computer as passing through the center of gravity of the distal third of the tibia model and minimizing the moment of inertia. The LM and MM could be directly determined from the reconstructed bone models by identifying their tips.

To describe the displacement of the talus, calcaneus, navicular, and cuboid bones in the hindfoot, the position and orientation of each bone needed to be precisely define. A local coordinate system (LCS) was established for each of the four hindfoot bones. The establishment of

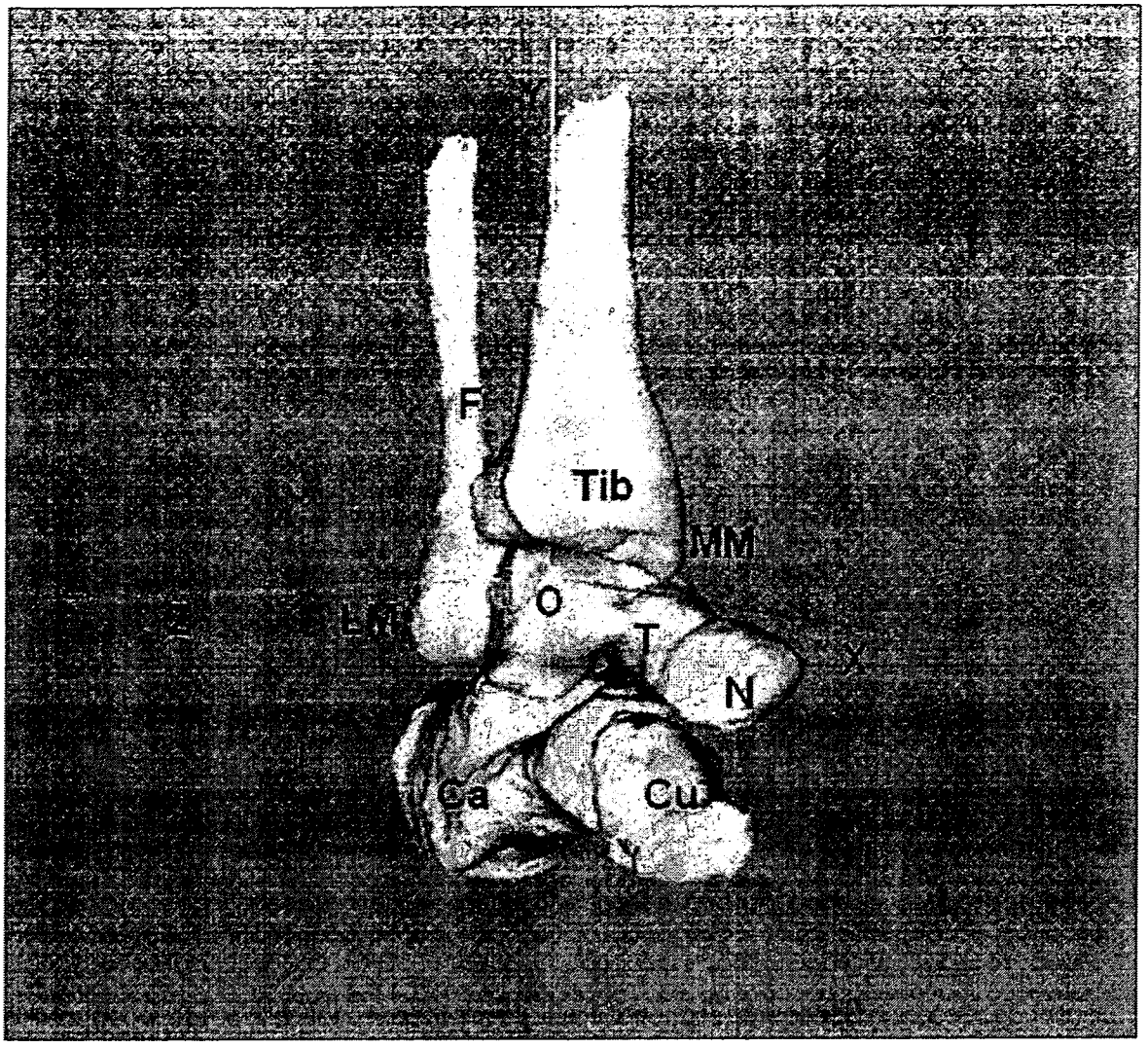

Figure 1. Establishing the standard coordinate system. Tib, tibia; F, fibula; T, talus; Ca, calcaneus; Cu, cuboid; N, navicular; O, origin; X, Y, and Z stand for the *x*-, *y*-, and *z*-axes of the standard coordinate system; LM, lateral malleoli; MM, medial malleoli.

the LCS was completed by the method of principal axes (x, y, z) and centroid (O). The principal axes were calculated by the software from the volume file and were orthogonal to each other and passing through the centroid. The position of the centroid plus the directions of the principal axes formed the mathematical representation and completely described the position and orientation of the bone in terms that could be further analyzed.[19] Because the orientation of the axes is dependent only on the shape of the bone surface, the LCS could be used as a set of markers attached to the bone.[20] However, the application of the LCS also depended on the stability of the principal axes within the bone. In other words, the principle axes should be stable within a bone regardless of whether the bone is normal or deformed by RA. Thus, the LCS could be used as a satisfactory marker set to analyze the displacement of the bone. Considering the dramatic change in shape of the bone surface in some RA patients, we modified the orientation of the axes using definite anatomical markers to make the axes more stable. The major principle axis was the basis of modification, because the major principal axis (long axis) was relatively stable and was used by Woodburn and colleagues to analyze hindfoot architecture in RA cases.[5] The origin and orientation of the LCS of each bone is shown in Figure 2.

For the calcaneus, the origin was the centroid of the calcaneus surface model, the x-axis was the long axis of the calcaneus in the forward direction, the z-axis lay in the plane defined by the x-axis and the centroid of the sustentaculum tali in the lateral direction, and the y-axis was perpendicular to the x-z plane in an upward direction. To obtain the centroid of the sustentaculum tali, the sustentaculum tali was cut off using unique

 DOI 10.1002/jor

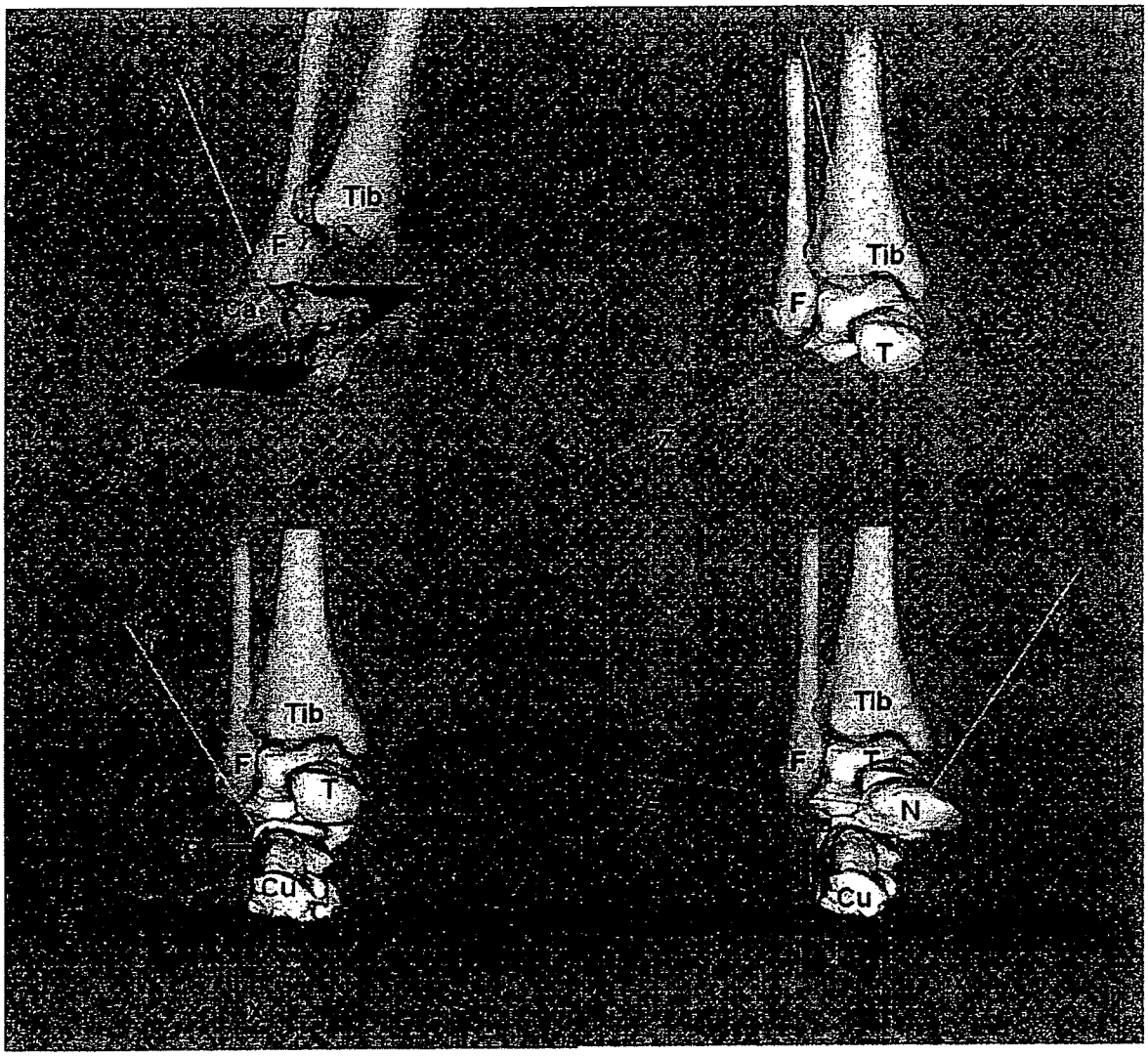

Figure 2. Establishing the local coordinate systems. Tib, tibia; F, fibula; T, talus; Ca, calcaneus; Cu, cuboid; N, navicular; R, ridge of the cuboid; S, sutentaculum tali of the calcaneus; O, origin is the centroid of the calcaneus surface model; X, Y, and Z stand for the X-, Y- and Z- axes of the local coordinate system.

software, and its bone model was reconstructed. The centroid position was determined by the software. The sustentaculum tali was then put back to its original position with the same software.

For the talus, the origin was the centroid of the talus surface model, the x-axis was the long axis of talus in the forward direction, the y-axis is perpendicular to the dome of the talus in an upward direction, and the z-axis was perpendicular to the x-y plane in a lateral direction. To determine the y-axis, a plane was passed through the centroid perpendicular to the x-axis. The line on the plane perpendicular to the dome of the talus was determined using unique software.

For the navicular, the origin was the centroid of the navicular surface model, the z-axis was the long axis of the navicular in a lateral direction, the y-axis was the middle axis with an upward direction, the x-axis was the shortest axis with a forward direction. The x-, y-, and z-axes were determined automatically by software calculations.

For the cuboid, the origin was the centroid of the cuboid surface model, the x-axis was the long axis of the cuboid in a forward direction, the y-axis passed through the ridge of the cuboid in an upward direction, and the z-axis was perpendicular to the x-y plane in a lateral direction. The ridge of the cuboid can be clearly identified from the bone model.

Once a stable LCS marker set was established for the talus, the centroid position and axes' orientation of the talus relative to the tibia (SCS) could be calculated. Three rotational parameters (Rx, Ry, Rz) and three translational parameters (Gx, Gy, Gz) were obtained by

the Eueler angle method. All translational parameters were normalized to the length between the LM and MM. By comparing the six parameters between groups, the displacement of the talus relative to the tibia was determined. A description of the displacement included the direction and amount of displacement of each bone's centroid, the orientation of rotation, and the amount of rotation.

The LCS matching method was used to analyze misalignments in the subtalar and midtarsal joints. The LCS of the RA talus was matched with that of the normal talus to analyze the displacements of the calcaneus and navicular in relation to the talus, which indicated the displacements in the subtalar and talonavicular joints, respectively. The LCS of the RA calcaneus was matched with that of the normal calcaneus to analyze the displacement of the cuboid relative to the calcaneus, which indicated the displacement in the cubocalcaneal joint. The LCS of the RA cuboid was matched with that of the normal cuboid to analyze the displacement of the navicular relative to the cuboid, which indicated the displacement in the cubonavicular joint.

The translational displacements along the *x*-, *y*-, and *z*-axes of the SCS were represented by *Gx*, *Gy*, and *Gz*, respectively. If any values increased in RA patients, the bone moved along the positive direction of the axis. Conversely, if any of these values decreased, the bone moved along the negative direction. *Rx*, *Ry*, and *Rz* denoted the rotational displacements around the *x*-, *y*-, and *z*-axes of the SCS, respectively. If these values increased in RA patients, the bone had varus rotation, adduction, and dorsal flexion, respectively. Conversely, if these values decreased, the bone showed valgus rotation, abduction, and plantar flexion.

The pattern of deformity was visualized using surface models created by a modified version of Visualization Toolkit software (Kitware Inc., New York, NY). The resulting calculated deformities were validated through animation made by the same software.

Validation of Accuracy

The accuracy of the methodology was determined in vitro. Three MR images and CT scans of a fresh cadaveric foot were acquired, only changing the direction of the MRI or CT slices. Segmentation and 3D reconstruction of the cuboid and calcaneus were conducted separately from each set of data, followed by the establishment of the LCSs of both bones. The relative position of the cuboid to the calcaneus was obtained using the LCS of each bone and compared among the three MRI or CT slices. The results in the MRI group showed a mean rotation error of $0.8° \pm 0.3°$ and a mean translation error of 0.04 ± 0.01 mm. In the CT group, the mean rotation error was $0.67° \pm 0.23°$ and the mean translation error was 0.03 ± 0.01 mm. Therefore, the experimental errors that might be caused by MRI or CT acquisition, segmentation, reconstruction, and establishment of an anatomical reference system were very small. The relative position of the cuboid to the calcaneus was also compared between the MRI and CT groups; the mean rotation error was $0.92° \pm 0.38°$, and the mean translation error was 0.08 ± 0.02 mm.

Statistical Analysis

Means and standard deviations were reported as descriptive statistics. A one-way MANOVA was conducted to determine if differences existed in the six parameters (*Gx*, *Gy*, *Gz*, *Rx*, *Ry*, and *Rz*) between the control and RA groups using SPSS software (ver. 12.0). A p value of less than 0.05 was considered significant.

RESULTS

Considering the displacement in the ankle joint (the talus relative to the tibia), the talus *Rz* decreased significantly ($p = 0.014$), so that the talus had plantar flexion relative to the tibia (Table 1). The rotation angle was 11° (Table 2, Fig. 3). For the displacements in the subtalar joint (the calcaneus relative to the talus) and the talonavicular joint (the navicular relative to the talus), the *Gy* and *Gz* of the calcaneus increased significantly ($p = 0.007$ and $p = 0.036$, respectively). The *Rx* of the calcaneus decreased significantly ($p < 0.0001$, Table 1). The increases of *Gy* and *Gz* demonstrated that the calcaneus translated laterally and upward in relation to the talus. The decrease of *Rx* indicated that the calcaneus had significant valgus rotation relative to the talus. The valgus angle was 10.5°, the lateral shift was about 3.9 mm, and the upward translation was 4.7 mm (Table 2, Fig. 3).

The *Rz*, *Gy*, and *Gz* of the navicular increased significantly ($p < 0.001$, $p = 0.001$, and $p = 0.002$, respectively). The *Rx* and *Ry* of the navicular decreased significantly ($p < 0.0001$ and $p = 0.006$, respectively; Table 1). The increases of *Rz*, *Gy*, and *Gz* indicated that the navicular flexed dorsally as well as translated upward and laterally in relation to the talus. The decreases of *Rx* and *Ry* demonstrated that the navicular had valgus rotation and abduction relative to the talus. The angles were 11.6° valgus rotation, 7.6° abduction, and 15.5° dorsal flexion. The upward and lateral translations were 4.3 mm and 4.8 mm, respectively (Table 2, Fig. 3).

For displacements in the cubocalcaneal joint (the cuboid relative to the calcaneus) and the cubonavicular joint (the navicular relative to the cuboid), the three translational parameters (*Gx*, *Gy*, and *Gz*) and the three rotational parameters (*Rx*, *Ry*, and *Rz*) of the cuboid relative to the calcaneus showed no significant differences

DOI 10.1002/jor

Table 1. Displacement of the Four Bones in the Hindfoot of Patients with Rheumatoid Arthritis

		RA ($n = 21$)		Normal ($n = 10$)		
	Parameters	Mean	SD	Mean	SD	p
Talus–tibia	*Gx* (mm)	7.8	1.9	8.0	1.9	0.86
	Gy (mm)	−8.3	2.3	−9.1	1.7	0.33
	Gz (mm)	−6.8	1.0	−7.4	0.5	0.08
	Rx (deg)	16.8	8.0	15.4	4.3	0.58
	Ry (deg)	27.9	7.8	31.0	3.0	0.22
	Rz (deg)	−34.1	14.1	−22.0	4.4	0.01*
Cal–talus	*Gx* (mm)	−7.9	3.9	−9.9	2.0	0.14
	Gy (mm)	−35.1	4.8	−39.8	2.2	0.007*
	Gz (mm)	9.7	5.3	5.8	2.7	0.04*
	Rx (deg)	8.7	6.6	20.5	6.3	< 0.0001*
	Ry (deg)	10.5	8.8	11.1	4.2	0.84
	Rz (deg)	20.4	10.9	15.2	4.1	0.16
Navi–talus	*Gx* (mm)	35.0	2.6	34.6	2.8	0.71
	Gy (mm)	−17.8	3.5	−22.2	2.3	0.001*
	Gz (mm)	−17.0	4.3	−21.9	2.4	0.002*
	Rx (deg)	−36.7	8.3	−21.5	7.1	< 0.0001*
	Ry (deg)	9.0	13.2	22.3	6.7	0.006*
	Rz (deg)	−24.8	6.6	−36.4	9.9	< 0.001*
Cubo–cal	*Gx* (mm)	37.7	1.8	39.0	3.5	0.18
	Gy (mm)	−38.5	3.1	−39.4	3.1	0.50
	Gz (mm)	5.2	2.5	3.8	2.0	0.110
	Rx (deg)	−6.5	7.3	−5.5	7.2	0.73
	Ry (deg)	−30.8	5.7	−28.6	5.6	0.33
	Rz (deg)	−25.7	10.4	−30.8	7.8	0.18
Navi–cubo	*Gx* (mm)	36.0	1.9	34.3	2.7	0.05
	Gy (mm)	−21.4	2.1	−22.1	2.6	0.40
	Gz (mm)	−20.4	1.3	−21.7	2.9	0.09
	Rx (deg)	−22.6	5.6	−21.6	6.9	0.66
	Ry (deg)	17.6	7.7	22.7	5.7	0.07
	Rz (deg)	−31.4	8.0	−36.2	9.7	0.16

Gx, *Gy*, *Gz* stand for the position of the centroid in SCS.
Rx, *Ry*, *Rz* stand for the rotational displacement of bone around the *x*-, *y*-, and *z*-axes of the SCS.
*p value shows significant difference.

between the two groups (all six p values > 0.05). No significant displacement was found in the cubocalcaneal joint of RA patients. The same results were obtained for the three translational (*Gx*, *Gy*, and *Gz*) and three rotational parameters (*Rx*, *Ry*, and *Rz*) of the navicular relative to the cuboid (all six p values > 0.05; Table 1), with no significant displacement in the cubonavicular joint of RA patients. Thus, the calcaneus, the cuboid, and the navicular might be displaced together in RA patients with RA and have no relative displacement among them (Fig. 4). All of the results above are shown in Animation 1.

Animation 1: The Talus showed planter flexion relative to the tibia. The calcaneus, cuboid, and navicular bones might have the same pattern of deformity.

DISCUSSION

The in vivo 3D technique used in this study could provide accurate, quantitative, readily visualized, and clinically meaningful information for skeletal misalignment of RA hindfoot valgus deformity. Although radiographic measurement is the usual method used to analyze RA hindfoot valgus deformity objectively, most previous studies concentrated on medial arch collapse and heel valgus deformity using 2D methods. Such analysis could not provide a complete 3D description of structural changes in the tarsal region of an RA foot. A few 3D studies have been conducted, but the parameters used were too complicated for use in clinical practice. In our study, translational and rotational displacements of each hindfoot bone was accurately

Table 2. Average Displacement from Normal Position to RA Displacement Position

		Rotation (deg)		Center of Gravity (mm)
Talus to tibia	*Rx*	4.4 varus	*Gx*	0.1 posterior
	Ry	0.3 abduction	*Gy*	0.8 upward
	Rz	11.0 plantar flexion*	*Gz*	0.6 lateral
Calcaneus to talus	*Rx*	10.5 valgus*	*Gx*	2.0 anterior
	Ry	2.2 abduction	*Gy*	4.7 upward*
	Rz	4.6 dorsal flexion	*Gz*	3.9 lateral*
Navicular to talus	*Rx*	11.6 valgus*	*Gx*	0.4 anterior
	Ry	7.6 abduction*	*Gy*	4.3 upward*
	Rz	15.5 dorsal flexion*	*Gz*	4.8 lateral*
Cuboid to calcaneus	*Rx*	1.5 valgus	*Gx*	1.3 posterior
	Ry	1.7 abduction	*Gy*	0.8 upward
	Rz	4.6 dorsal flexion	*Gz*	1.5 lateral
Navicular to cuboid	*Rx*	3.7 valgus	*Gx*	1.7 anterior
	Ry	2.5 abduction	*Gy*	0.7 upward
	Rz	5.1 dorsal flexion	*Gz*	1.3 lateral

*p value shows significant difference.

described. The six parameters (*Gx*, *Gy*, *Gz*, *Rx*, *Ry*, and *Rz*) obtained using this technique are relatively simple and practical. In addition, the animation permitted good visualization of the deformity pattern, which might be beneficial in understanding the deformity pathomechanism. The number of abnormal parameters and the extent to which they deviated from normal gave a composite measurement of the severity of the deformity. Furthermore, the pattern of misalignment and the extent of displacement could be used for preoperative planning and reasonable surgical treatment.

Our results also confirmed the pathomechanism of RA hindfoot valgus deformity. Pes planovalgus is the most frequent deformity of the RA middle and hindfoot.[1,6] Changes in the subtalar and talonavicular joints are believed to dominate.[4] The presumed pathomechanism seems to be stress-related mechanical changes resulting from weakened ligaments.[4] RA causes severe inflammation of the talonavicular joint and the tarsal sinus, on the deep surface of which the strong plantar calcaneonavicular ligament rests. Diffuse inflammation in these areas alters the statics of the foot as a whole.[6] When the medial arch does not tolerate weightbearing, 'the head of the talus falls down toward the medial side...in the plantar direction,'[2,6] and the calcaneus becomes deformed in a valgus direction, so the arch collapses and flatfoot occurs.

In our study, the talus flexed in the plantar direction, and the calcaneus showed a lateral, upward shift and valgus rotation. The displacements of the talus and calcaneus correspond to the pathomechanism described above. The stretch or disruption of the strongest interosseous ligament in the tarsal sinus should be considered.

Based on our results, talonavicular joint deformity and talar tilting may contribute to the mechanism of medial longitudinal arch collapse. Vanio believed that the break of the medial longitudinal arch is more frequent in the naviculocuneiform joint than in the talonavicular joint.[21] In contrast, Vahvanen described the talonavicular joint as the site of the crucial change producing flat foot and splay foot.[6] The navicular is elevated and displaced laterally, and consequently the head of the talus falls down towards the medial side of the foot in the plantar direction.[6] Gross and colleagues reported that navicular tuberosity displacement or drop may reflect excessive subtalar joint pronation, due to insufficient support of the medial longitudinal arch from ligaments and tendons.[22] Navicular displacement also indicates the degree to which the talus plantarly flexes in the space on the calcaneus that is stabilized during subtalar pronation.[23]

Our study is the first to report that the navicular bone showed valgus rotation, abduction, and dorsal flexion and translated upwardly and laterally relative to the talus. Combined with plantar flexion of the talus, the medial arch height decreased and medial bulging of the talonavicular joint occurred. The navicular tuberosity displacement or navicular drop was also seen using animation. Therefore, the talonavicular joint might be a key point of medial arch collapse. Further study on the

 DOI 10.1002/jor

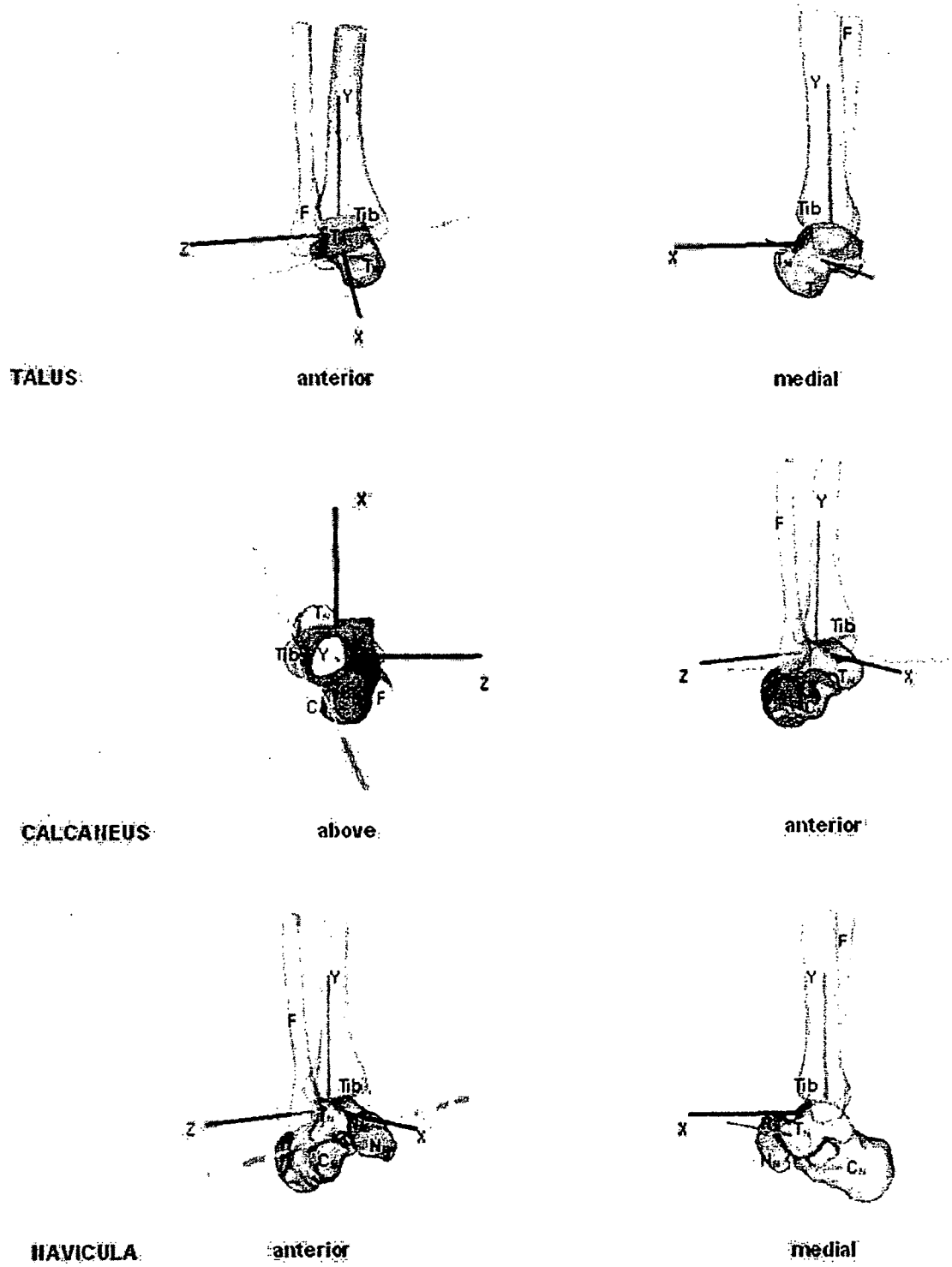

Figure 3. Displacements of the talus, calcaneus, and navicular bones. Tib, tibia; F, fibula; T_N, normal talus; T_R, RA talus; C_N, normal calcaneus; C_R, RA calcaneus; N_N, normal navicular; N_R, RA navicular; X, Y, and Z stand for the *x*-, *y*-, and *z*-axes of the standard coordinate system.

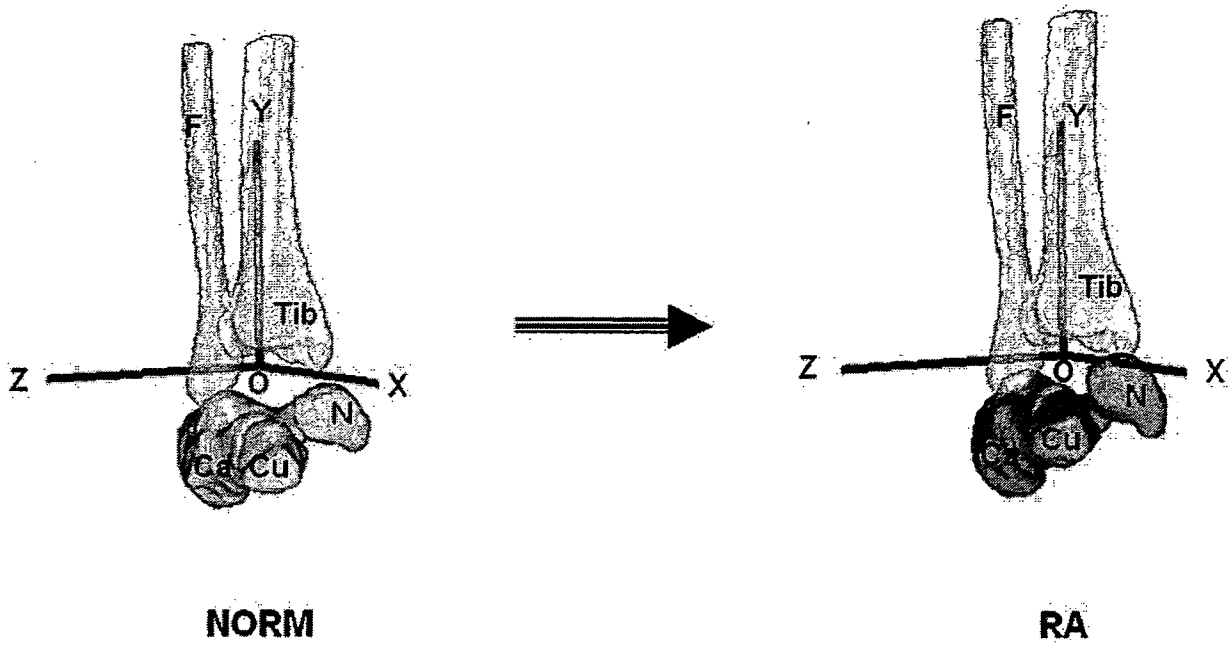

Figure 4. The calcaneus, cuboid, and navicular bones move in the same way. Tib, tibia; F, fibula; Ca, calcaneus; Cu, cuboid; N, navicular; O, origin; X, Y, and Z stand for the *x*-, *y*-, and *z*-axes of the standard coordinate system.

change in the naviculocuneiform joint is recommended.

The relationships among the cuboid, calcaneus, and navicular bones, reported here for the first time, might be helpful in surgical treatment of RA hindfoot valgus deformity. The cuboid showed no displacement relative to the calcaneus, and the navicular had no relative displacement to the cuboid, suggesting that the calcaneus, the cuboid, and the navicular might move in the same pattern. This is supported by findings that the hindfoot valgus deformity in RA patients primarily occurred in the subtalar and talonavicular joints.[4,24] The result might be useful for surgical treatment, because it suggests that in some circumstances, cuboid correction is unnecessary. Double arthrodesis (of the subtalar and talonavicular joints) rather than triple arthrodesis should be more often recommended for patients with RA hindfoot valgus deformity.

Our study is limited by the age mismatch between the patients with RA and the controls. On the other hand, our study was designed to compare the feet deformed by RA with normal feet. Many older people have normal feet, but they may have other deformities caused by OA or diseases such as flat foot, which sometimes is asymptomatic. These conditions make those older people unsuitable as controls. Conversely, not all young people have normal skeletal alignments. However, most young people are suitable as controls. We could not perform CT scans on normal subjects because of the radiation issue. CT resolution for bone is superior to that of MRI. During segmentation, the marching cubes algorithm worked better with CT than with MRI bone margins. However, we believe that ample information is retained using MRI, if geometric properties of a normal bone are desired, such as the calculated geometric centroid and principle axes. In this respect, MRI appears comparable to CT. The difference in accuracy between the MRI and CT groups was very small by validation. Functional CT and MRI of the foot under body-weight loading are desirable, but difficult to achieve.

ACKNOWLEDGMENTS

H. B. Liu was a research fellow sponsored by the Japan–China Medical Association. This work was supported by a Japan–China Sasagawa Medical Scholarship. The authors thank Hisao Moritomo, Guixing Qiu, Wataru Sahara, Kunihiro Oka, Takahiro Ishii, Ryutaro Fujii, Akira Goto, and Ryoji Nakao for their invaluable contributions to the experimental procedure.

REFERENCES

1. Bouysset M, Bonvoison B, Lejeune E, et al. 1987. Flattening of the rheumatoid foot in tarsal arthritis on X-ray. Scand J Rheumatol 16:127–133.

DOI 10.1002/jor

2. Bouysset M, Tebib JG, Weil G, et al. 1987. Deformation of the adult rheumatoid rearfoot: a radiographic study. Clin Rheumatol 6:539–544.
3. Michelson J, Easley M, Wigley FM, et al. 1994. Foot and ankle problems in rheumatoid arthritis. Foot Ankle Int 15: 608–613
4. Spiegel TM, Spiegel JS. 1982. Rheumatoid arthritis in the foot and ankle — diagnosis, pathology, and treatment: the relationship between foot and ankle deformity and disease duration in 50 patients. Foot Ankle 2:318–324.
5. Woodburn J, Udupa KJ, Hirsch BE, et al. 2002. The geometric architecture of the subtalar and midtarsal joints in rheumatoid arthritis based on magnetic resonance imaging. Arthritis Rheum 46:3168–3177.
6. Vahvanen VA. 1967. Rheumatoid arthritis in the pantalar joints: a follow-up study of triple arthrodesis on 292 adult feet. Acta Orthop Scand Suppl 112–119.
7. Keenan MA, Peabody TD, Gronley JK, et al. 1991. Valgus deformities of the feet and characteristics of gait in patients who have rheumatoid arthritis. J Bone Joint Surg Am 73:237–247.
8. Seltzer SE, Weissman BN, Braunstein EM, et al. 1985. Computed tomography of the hindfoot with rheumatoid arthritis. Arthritis Rheum 28:1234–1242.
9. Montagne J, Chevrot A, Galmiche JM. 1981. Atlas of foot radiology. New York: Masson Publishing USA.
10. Saltzman CL, Brandser EA, Berbaum KS, et al. 1994. Reliability of standard foot radiographic measurements. Foot Ankle Int 15:661–665.
11. Seltzer SE, Weissman BN, Braunstein EM, et al. 1984. Computed tomography of the hindfoot. J Comput Assist Tomogr 8:488–497.
12. Ishii T, Mukai Y, Hosono N, et al. 2004. Kinematics of the upper cervical spine in rotation: in vivo three-dimensional analysis. Spine 29:E139–E144.
13. Ishii T, Mukai Y, Hosono N, et al. 2004. Kinematics of the subaxial cervical spine in rotation: in vivo three-dimensional analysis. Spine 29:2826–2831.
14. Goto A, Moritomo H, Murase T, et al. 2005. In vivo three-dimensional wrist motion analysis using magnetic resonance imaging and volume-based registration. J Orthop Res 23:750–756.
15. Moritomo H, Goto A, Sato Y, et al. 2003. The triquetrum-hamate joint: an anatomic and in vivo three-dimensional kinematic study. J Hand Surg (Am) 28:797–805.
16. Itohara T, Sugamoto K, Shimizu N, et al. 2005. Assessment of the three-dimensional relationship of the ossific nuclei and cartilaginous anlagen in congenital clubfoot by 3-D MRI. J Orthop Res 23:1160–1164.
17. Lorensen WE, Cline HE. 1987. Marching cubes: a high resolution 3D surface construction algorithm. Comput Graphics 21:163–169.
18. Cappozzo A, Catani F, Croce UD, et al. 1995. Position and orientation in space of bones during movement: anatomical frame definition and determination. Clin Biomech 10:171–178.
19. Hirsch BE, Udupa JK, Samarasekera, S. 1996. New method of studying joint kinematics from three-dimensional reconstructions of MRI data. J Am Podiatric Med Assoc 86:4–15.
20. Stindel E, Udupa JK, Hirsch BE, et al. 2001. An in vivo analysis of the motion of the peritalar joint complex based on MR imaging. IEEE Trans Biomed Eng 48:236–247.
21. Vainio K. 1956. The rheumatoid foot: a clinical study with pathological and roentgenological comments. Ann Chir Gynec 45(Suppl 1):1–107.
22. Gross MT. 1995. Lower quarter screening for skeletal malalignment — suggestions for orthotics and shoewear. J Orthop Sports Phys Ther 21:389–405.
23. Picciano AM, Rowlands MS, Worrell T. 1993. Reliability of open and closed kinetic chain subtalar joint neutral positions and navicular drop test. J Orthop Sports Phys Ther 18:553–558.
24. Cimino WG, O'Malley MJ. 1998. Rheumatoid arthritis of the ankle and hindfoot. Orthop Clin North Am 24:157–172.

Clin Rheumatol (2007) 26: 515–519
DOI 10.1007/s10067-006-0318-y

ORIGINAL ARTICLE

Takashi Kitamura · Jun Hashimoto · Tsuyoshi Murase · Tetsuya Tomita · Takako Hattori · Hideki Yoshikawa · Kazuomi Sugamoto

Radiographic study of joint destruction patterns in the rheumatoid elbow

Received: 7 January 2006 / Revised: 1 April 2006 / Accepted: 3 April 2006 / Published online: 3 May 2006

Abstract Knowledge of the pattern of joint destruction is important for planning the therapeutic approach to rheumatoid arthritis (RA) of the elbow. Accordingly, we carried out a large-scale radiographic study with the objective of elucidating the joint destruction pattern in rheumatoid elbows. From 2001 through 2003, we examined and took plain X-rays of both elbows of 193 RA patients (i.e., 386 elbows), consisting of 18 men and 175 women, with a mean age of 57.0 years. Radiographic images of the elbow joints were used to classify the degree of bone loss in various zones on the elbow joint surface into four grades of severity, and joint destruction was compared between the left and right elbows. In addition, correlation in the extent of bone loss between each of the zones of the same elbow and differences in the extent of bone loss were analyzed statistically. The results showed direct correlations for destruction of the elbow joint surface among the zones for the left and right elbow joints and in the same elbow joint. However, more severe destruction was observed on the radial side of the humeral trochlea, and it was surmised that destruction of the elbow joint must begin at that site and gradually spread mediolaterally. In addition, in the same elbow joint, the correlation in the degree of bone loss between the trochlea of humerus and the trochlear notch was especially strong, indicating that the bone destruction at both sites represented mirror lesions. We conclude that when performing radiographic diagnosis of the joint damage in the rheumatoid elbow, knowledge of this pattern of joint destruction will be useful for assessing whether there is joint destruction in the initial stage and for deciding the therapeutic approach.

Keywords Elbow joint · Radiography · Rheumatoid arthritis

T. Kitamura (✉)
Department of Orthopedic Surgery, Kaizuka City Hospital,
3-10-20, Hori, Kaizuka,
Osaka 597-0015, Japan
e-mail: kitamura@tb3.so-net.ne.jp
Tel.: +81-0724-225865
Fax: +81-0724-396061

J. Hashimoto · T. Murase · T. Tomita ·
H. Yoshikawa · K. Sugamoto
Department of Orthopaedics,
Osaka University Medical School,
2-2, Yamadaoka, Suita,
Osaka 565-0871, Japan

T. Hattori
Department of Orthopedic Surgery, NTT West Osaka Hospital,
2-6-40,Karasugatsuji,Tennouji,
Osaka 543-8922, Japan

Introduction

The elbow joint is a common site for the development of rheumatoid arthritis (RA), and it is one of the most important joints in the upper limb as it controls the reach of the hand [1–4]. For this reason, disorders of the elbow joint can seriously interfere with activities of daily living (ADL) of RA patients. In general, when arthropathy is mild, therapy consists of conservative treatments such as drug administration and/or intraarticular injection of steroid. In severe disease, surgical treatments such as synovectomy and artificial elbow joint replacement may be performed [1–4]. For treatment selection and planning, it is very important for the physician to have a good understanding of the pattern of destruction that has occurred in the RA elbow joint. However, it is unfortunate that to date very few reports of analysis of the pattern of bone destruction in RA elbow joints have been published.

We therefore carried out a large-scale radiographic study with the objective of elucidating the pattern of RA elbow joint bone destruction.

Subjects

From 2001 to 2003, we examined plain X-rays of both elbow joints of 233 patients who satisfied the ARA diagnostic criteria. Forty of these patients were excluded from the present study due to previous synovectomy or

artificial elbow joint replacement (33 patients) or because the X-rays were unreadable (seven patients). The remaining 193 RA patients, i.e., 386 elbows, were the subjects of this study. They consisted of 18 men and 175 women, with an age range of 23~84 years (mean 57.0 years). History of drug administration, including steroids, and duration of RA were unclear.

Methods

Radiographic classification of the severity of RA was performed on the basis of plain X-ray anteroposterior images and lateral images of the bilateral elbow joints that were obtained for each patient at the time of final examination. X-rays were taken with the patient in a sitting position. Frontal views were obtained with the elbow joint extended and the forearm in the supine position, while lateral views were obtained with the elbow joint flexed at 90° and the forearm in the intermediate position. The frontal images were divided into three zones: the capitulum of the humerus (zone A), the radial side of the humeral trochlea (zone B), and the ulnar side of the humeral trochlea (zone C). The extent of destruction of the joint surface was determined for each of these zones. In addition, from the lateral view, the extent of joint surface destruction was determined for the olecranon (zone D).

Extent of joint destruction was assessed by reference to a template of the normal elbow joint that had been prepared in advance. The ratings used were grade 0, no bone loss; grade 1, less than 3 mm of bone loss from the joint surface; grade 2, bone loss of 3 to less than 6 mm; and grade 3, bone loss of 6 or more mm (Figs. 1 and 2).

We investigated the extent of bone destruction observed in each of the joint zones, and also investigated whether there was any correlation in destruction among the zones. In practice, we first investigated the correlation in the extent of bone loss in the same zone in both elbows of the same patient, and then compared joint destruction in the left and right elbows. In addition, the correlation in the extent of bone loss among each zone of the same elbow and differences in the extent of bone loss were analyzed statistically.

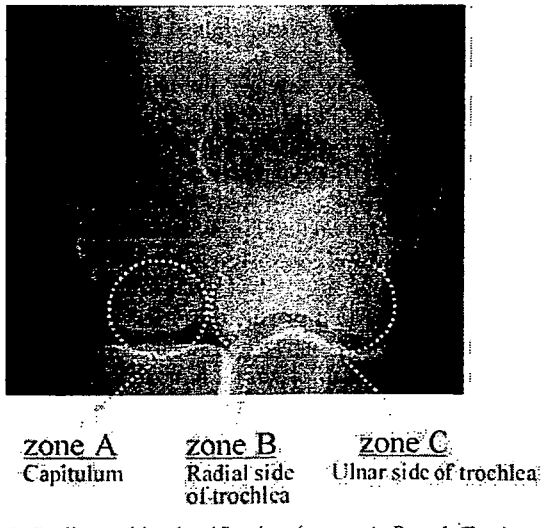

Fig. 1 Radiographic classification (*zones A, B,* and *C*)

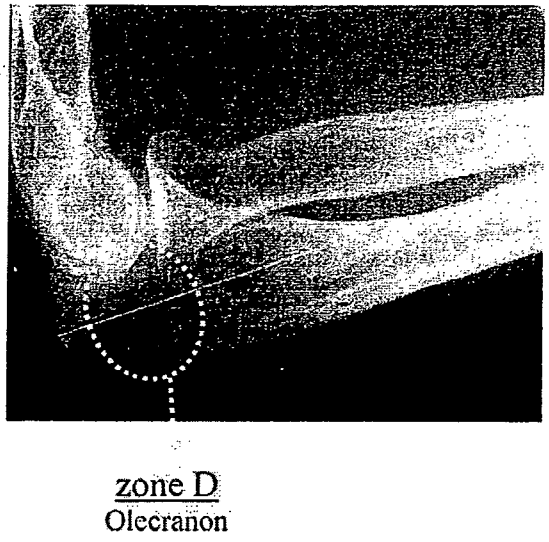

Fig. 2 Radiographic classification (*zone D*)

Spearman's ranked correlation coefficients were used for statistical analyses of correlations, while one-way analysis of variance (ANOVA) and Fisher's least significant difference (LSD) test were used to analyze differences in extent of bone loss.

Results

The extent of bone loss in each zone of the joint as seen on frontal X-ray images was as follows: zone A, 26.2% grade 0, 62.1% grade 1, 8.8% grade 2, and 2.8% grade 3; zone B, 26.2% grade 0, 37.0% grade 1, 26.9% grade 2, and 9.8% grade 3; and zone C, 26.9% grade 0, 62.1% grade 1, 2.6% grade 2, and 8.3% grade 3. The extent of bone loss was therefore similar in zone A and zone C, whereas zone B exhibited a lower percentage rated as grade 2 and a higher percentage rated as grade 3 compared with the other two zones. The extent of bone loss seen on lateral X-ray images (zone D) was grade 0 in 27.2%, grade 1 in 61.1%, grade 2 in 8.3%, and grade 3 in 3.4% (Table 1).

A significant correlation was found for the extent of bone loss in the same zone between the left and right elbows, and correlation was found for bilateral elbow joint destruction (zone A r=0.833, p<0.001; zone B r=0.804, p<0.001; zone C r=0.881, p<0.001; and zone D r=0.887, p<0.001).

In addition, statistically significant correlations were also found for the extent of bone loss among zones in the same elbow (r=0.789~0.951, p<0.001) (Fig. 3). A particularly strong correlation was demonstrated between zone C and zone D (r=0.951, p<0.001).

On the other hand, the extent of bone loss was significantly greater in zone B compared with zone A and zone C (p<0.05), indicating that joint surface

Table 1 Radiographic classification of severity of joint destruction in the elbow (n=193)

Grade	Zone A		Zone B		Zone C		Zone D	
	R/L	Total(%)	R/L	Total(%)	R/L	Total(%)	R/L	Total(%)
0	50/51	26.2	49/52	26.2	51/53	26.9	51/54	27.2
1	123/117	62.2	73/70	37.1	120/120	62.2	117/119	61.1
2	14/20	8.8	54/50	26.9	7/3	2.6	16/16	8.3
3	6/5	2.8	17/21	9.8	15/17	8.3	9/4	3.4
Total	193/193	100	193/193	100	193/193	100	193/193	100

destruction was more advanced in the central part of distal humerus articular surface than at other sites (Fig. 4).

In addition, bone destruction of the humeral trochlea that extended to the olecranon fossa, i.e., a so-called Y-shaped

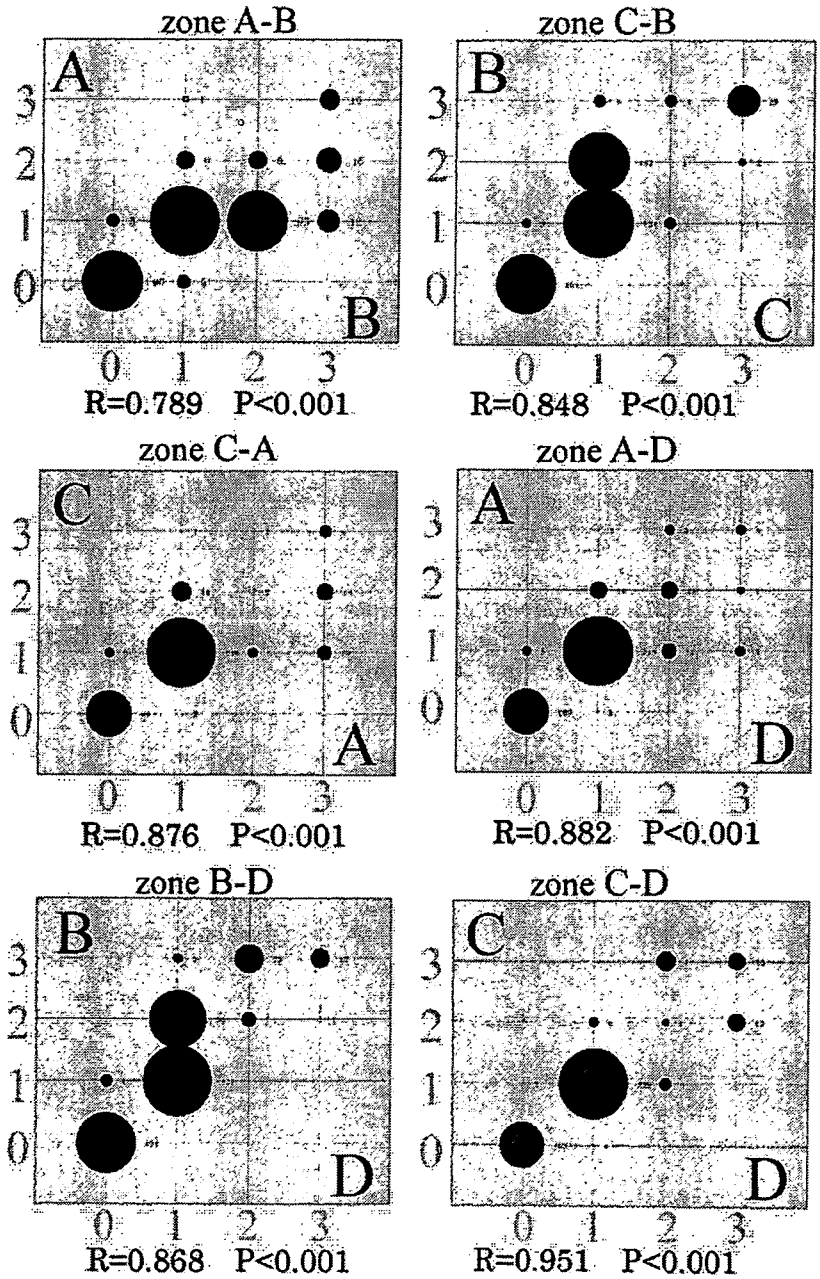

Fig. 3 Correlation of joint destruction among *zonesA*, *B*, *C*, and *D* (386 joints)

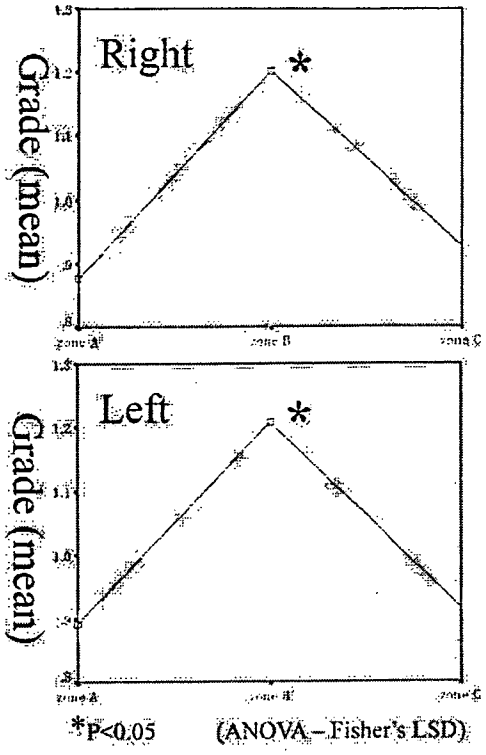

Fig. 4 Distribution of joint destruction grade (*zones A, B,* and *C*)

deformity, was observed in six of the patients, although this was bilateral in only two patients.

Discussion

Larsen's classification, based on the radiological findings for each joint, is widely used as an index of progression of RA disease stage. However, this classification has only two assessment criteria, i.e., the presence/absence of joint space narrowing and the presence/absence of joint surface erosion; the extent of bone loss is not assessed. Accordingly, this classification is said to have poor sensitivity for assessing the extent of joint destruction [5–7]. Lehtinen et al. [7] reported that joint space narrowing in the RA elbow differs from that in weight-bearing joints in that it occurs only subsequent to erosive destruction. They also stated that caution is necessary when using Larsen's classification to assess bone destruction in the elbow because it is a nonweight-bearing joint. In addition, joint destruction in RA is reported to generally show left–right symmetry [5–7]. However, that conclusion has been based only on simple bilateral comparison of the presence/absence of joint destruction, and, to date, there have been no reports of statistical analysis of site and extent of joint destruction. Accordingly, we carried out the present large-scale radiographic study with the objective of elucidating the pattern of bone destruction in the RA elbow joint. To achieve this, we used our own classification system to assess the extent of bone loss in various zones on the elbow joint surface, and joint destruction was compared between the left and right elbows. We then performed statistical analyses to determine whether there were any correlations in the extent of bone loss among each of the zones in the bilateral elbows and in the same elbow.

Our patients showed positive correlations among each of the zones for the extent of bone loss in the same elbow joint, and positive correlations were also found for the extent of joint surface bone loss in the same zones in the bilateral elbows. On the other hand, when we investigated the extent of bone loss in each zone in the same joint, we found it to be significantly greater on the radial side of the humeral trochlea compared with the ulnar side of the trochlea and the capitulum. We therefore surmised that the joint destruction must begin at the radial side of the humeral trochlea and gradually spread mediolaterally. In addition, in the same elbow joint, the correlation in the degree of bone loss between the ulnar side of the trochlea and the olecranon was particularly strong, indicating that the bone destruction at both sites represented symmetrical lesions.

Two theories have been proposed in an attempt to explain the underlying mechanism of the destruction observed in upper limb joints with RA. In the first, the principal cause is considered to be destruction and absorption of cartilage and bone as a result of the actions of cytokines released from the synovial tissue [8, 9]. The second theory holds that the major effects arise from anatomical and/or mechanical factors [10]. Ochi et al. [11] reported that even in the same joint the mechanism of destruction varies widely depending on the disease type. That is, they found that in the type involving damage to the smaller joints, the main bone destruction consisted of erosion of the joint surface due to proliferation of synovitis. Whereas with the mutilating type of arthritis, the main cause of bone destruction was crushing of bone that had become highly osteoporotic because of severe joint instability due to joint laxity.

It is possible that the level of stress applied to the elbow joints differs between the dominant and nondominant arm. However, in the present study, we found no clear left–right difference in the extent of joint destruction, suggesting that the effects of mechanical factors on bone destruction in the RA elbow are slight. Even so, consideration must be given to the fact that most of the patients in our present series were at an earlier stage of the disease, showing a milder degree of joint destruction. Conversely, however, some patients with severe joint destruction, such as is likely to cause the so-called Y-shaped deformity, exhibited clear left–right differences in the extent of damage. Therefore, we cannot rule out the possibility that mechanical factors play a larger role than immunological factors in the advanced stages of joint destruction.

Application of axial compression in the direction of the long axis of the forearm reportedly results in almost equal transmission of the force to the radial joint and the ulnar joint, or slightly greater transmission to the radial joint [12–14]. The surface of the radial side of the humeral trochlea becomes the varus–valgus pivot point of the elbow [15], and for this reason it is possible that when joint laxity occurs due to synovitis, forces are concen-

trated in that area and this leads to the progression of joint destruction.

Our present results indicated the possibility that joint destruction in the RA elbow begins on the radial side of the humeral trochlea and gradually spreads mediolaterally. If we accept the validity of this pattern of destruction of the elbow joint, then when analyzing X-rays taken in the early stage of RA elbow joint damage, it should be possible to focus on the radial side of the humeral trochlea and determine whether joint destruction had already begun. In addition, if bone destruction on the radial side of the trochlea were mild, we would be able to conclude that the joint destruction was at an early stage and that a minimally invasive therapy such as synovectomy was indicated.

The progression of joint destruction can be considered influenced by various factors, such as medication (including NSAIDs, DMARDs, and steroids), disease duration, and progression of joint deformation due to aging or osteoporosis [16–19]. A limitation of the present study was that we were unable to discuss the possible effects of drug treatments, disease duration, and aging in our patient series. However, this is the first report of a statistical analysis of the pattern of joint destruction in the rheumatoid elbow, and we think that our findings will make a significant contribution to decision making regarding therapeutic approaches to RA of the elbow.

References

1. Boyd AD, Thornhill TS (1989) Surgical treatment of the elbow in rheumatoid arthritis. Hand Clin 5(4):645–655
2. Rosenberg GM, Tuner RH (1984) Nonconstrained total elbow arthroplasty. Clin Orthop 187:154–162
3. Linclau LA, Winia WPCA, Korst JK (1983) Synovectomy of the elbow in rheumatoid arthritis. Acta Orthop Scand 54 (6):935–937
4. Pritchard RW (1991) Total elbow joint arthroplasty in patients with rheumatoid arthritis. Semin Arthritis Rheum 21(1):24–29
5. Ljung P, Jonsson K, Rydgren L, Rydholm U (1995) The natural course of rheumatoid elbow arthritis: a radiographic and clinical five-year follow up. J Orthop Rheumatol 8:32–36
6. Lehtinen JT, Kaarela K, Kauppi MJ, Belt EA, Maenpaa HM, Lehto MUK (2002) Bone destruction patterns of the rheumatoid elbow: a radiographic assessment of 148 elbows at 15 years. J Shoulder Elbow Surg 11:253–258
7. Lehtinen JT, Kaarela K, Belt EA, Kauppi MJ, Skytta E, Kuusela PP, Kautiainen HJ, Lehto MUK (2001) Radiographic joint space in rheumatoid elbow joints. A 15-year prospective follow-up study in 74 patients. Rheumatology 40:1141–1145
8. Kirwan JR (1997) The relationship between synovitis and erosions in rheumatoid arthritis. Br J Rheumatol 36:225–228
9. Cuomo F, Greller MJ, Zuckerman JD (1998) The rheumatoid shoulder. Rheum Dis Clin North Am 24:67–82
10. Tan AL, Tanner SF, Conaghan PG, Radjenovic A, O'Connor P, Brown AK, Emery P, McGonagle D (2003) Role of metacarpophalangeal joint anatomic factors in the distribution of synovitis and bone erosion in early rheumatoid arthritis. Arthritis Rheum 48:1214–1222
11. Ochi T, Iwase R, Yonemasu K, Matsukawa M, Yoneda M, Yukioka M, Ono K (1988) Natural course of joint destruction and fluctuation of serum C1q levels in patients with arthritis. Arthritis Rheum 31:37–43
12. Amis AA, Dowson D, Wright V, Miller JH (1979) The derivation of the elbow joint forces and their relation to prosthesis design. J Med Eng Technol 3:229–234
13. Amis AA, Dowson D, Wright V (1980) Elbow joint force predictions for some strenuous isometric actions. J Biomech 13:765–775
14. Halls AA, Travill R (1964) Transmission of pressure across the elbow joint. Anat Rec 150:243–247
15. Morrey BF, An KN, Stormont TJ (1988) Force transmission through the radial head. J Bone Jt Surg 70-A:250–256
16. McIlwain HH (2003) Glucocorticoid-induced osteoporosis: pathogenesis, diagnosis, and management. Prev Med 36:243–249
17. Solomon DH, Levin Elaine, Helfgott SM (2000) Patterns of medication use before and after bone densitometry: factors associated with appropriate treatment. J Rheumatol 27:1496–1500
18. Minaur NJ, Kounail D, Vedi S, Compston JE, Beresford JN, Bhalla K (2002) Methotrexate in the treatment of rheumatoid arthritis. II. In vivo effects on bone mineral density. Rheumatology 41:741–749
19. Dolan AL, Moniz C, Abraha H, Pitt P (2002) Does active treatment of rheumatoid arthritis limit disease-associated bone loss? Rheumatology 41:1041–1047

A three-dimensional quantitative analysis of carpal deformity in rheumatoid wrists

S. Arimitsu,
T. Murase,
J. Hashimoto,
K. Oka,
K. Sugamoto,
H. Yoshikawa,
H. Moritomo

From Osaka University Graduate School of Medicine, Osaka, Japan

We have measured the three-dimensional patterns of carpal deformity in 20 wrists in 20 rheumatoid patients in which the carpal bones were shifted ulnarwards on plain radiography. Three-dimensional bone models of the carpus and radius were created by computerised tomography with the wrist in the neutral position. The location of the centroids and rotational angle of each carpal bone relative to the radius were calculated and compared with those of ten normal wrists.

In the radiocarpal joint, the proximal row was flexed and the centroids of all carpal bones translocated in an ulnar, proximal and volar direction with loss of congruity. In the midcarpal joint, the distal row was extended and congruity generally well preserved. These findings may facilitate more positive use of radiocarpal fusion alone for the deformed rheumatoid wrist.

The most common deformity of the wrist in rheumatoid arthritis (RA) has been described as carpal supination with ulnar translocation[1] and many reports have attempted to evaluate this deformity.[2-8] However, they have been two-dimensional studies based generally on radiological assessment, the value of which is limited because the complex, overlapping appearance makes measurement difficult, especially in wrists with severe deformity. We have therefore undertaken an analysis of such deformities using a new three-dimensional (3D) technique.

Patients and Methods

We studied 20 wrists in 20 rheumatoid patients in which there was ulnar translocation on the anteroposterior radiograph. We chose wrists with a carpal-ulnar distance ratio below 0.27[9] and in which the shape of each bone was easily recognisable (Fig. 1). There were 19 women and one man with a mean age of 61 years (21 to 80). The mean duration of the disease was 15 years (6 to 38). A total of 18 patients had the more erosive subset of the disease, one the least erosive[10] and one juvenile RA. For comparison, we also chose a control group of ten normal wrists in ten men with a mean age of 41.4 years (18 to 76).

Imaging. Computerised tomography (CT) with a slice thickness of 0.625 mm was undertaken on a clinical helical-type scanner (LightSpeed Ultra16; General Electric, Maukesha, Wisconsin). During image acquisition, the wrists were in the neutral position with the axes of the third metacarpal and forearm aligned. The data were saved in a standard format (DICOM; Digital Imaging and Communications in Medicine).

Segmentation and construction of three-dimensional surface bone models. Segmentation is the extraction of individual bony regions. The anatomy or region of interest must be delineated and separated so that it can be viewed individually and 3D models reconstructed. Regions of individual bones were segmented semi-automatically using a software program for image analysis (Virtual Place-M; AZE Ltd, Tokyo, Japan). Surface models of the radius and each carpal bone were obtained by 3D surface generation of the bone cortex.[11-13]

Measurement of centroid translocation and carpal rotation. First, the position of the volume centroid of any bone was calculated from the CT files.[14] In order to measure the translocation, we defined the grid for the lower radius and each carpal bone within it. This was the orthogonal reference system originally advocated by Belsole et al[15] (Figs 2 and 3). For the radius this was determined as follows: The Y axis was the longitudinal radial axis and indicated the proximal (+)/distal (-) direction; the Z axis was the line through the styloid perpendicular to the Y axis and indicated radial (+)/ulnar (-) displacement; the X axis was the

* S. Arimitsu, MD, Orthopaedic Surgeon
* T. Murase, MD, PhD, Assistant Professor
* J. Hashimoto, MD, PhD, Associate Professor
* K. Oka, MD, Orthopaedic Surgeon
* K. Sugamoto, MD, PhD, Professor
* H. Yoshikawa, MD, PhD, Professor
* H. Moritomo, MD, PhD, Assistant Professor
Department of Orthopaedic Surgery
Osaka University Graduate School of Medicine, 2-2, Yamada-oka, Suita, Osaka 565-0871, Japan.

Correspondence should be sent to Dr S. Arimitsu; e-mail: sayu@df6.so-net.ne.jp

doi:10.1302/0301-620X.89B4.18476 $2.00

J Bone Joint Surg [Br] 2007;89-B:490-4.
Received 31 July 2006; Accepted after revision 5 December 2006

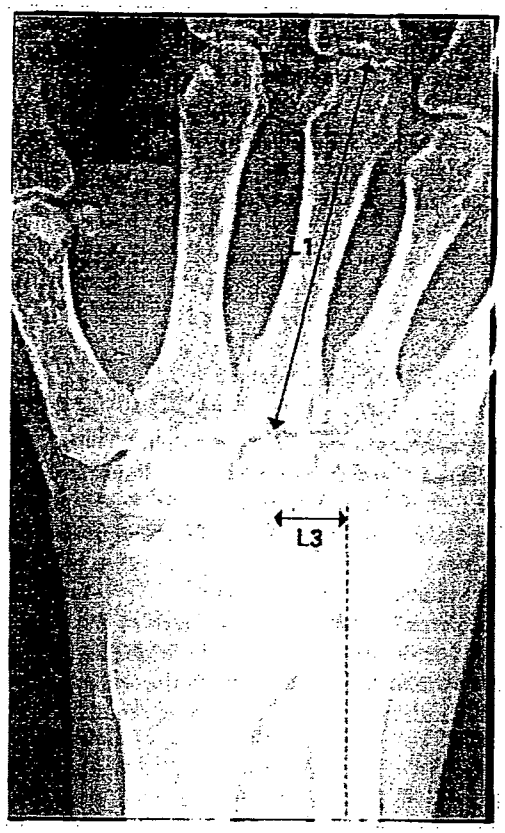

Fig. 1

Radiograph showing measurement of the carpal-ulnar distance ratio. It is calculated as L3/L1 where L3 is the distance between the centre of the capitate and the bony axis of the ulna and L1 the length of the third metacarpal. The normal ratio is 0.3 so 0.03.

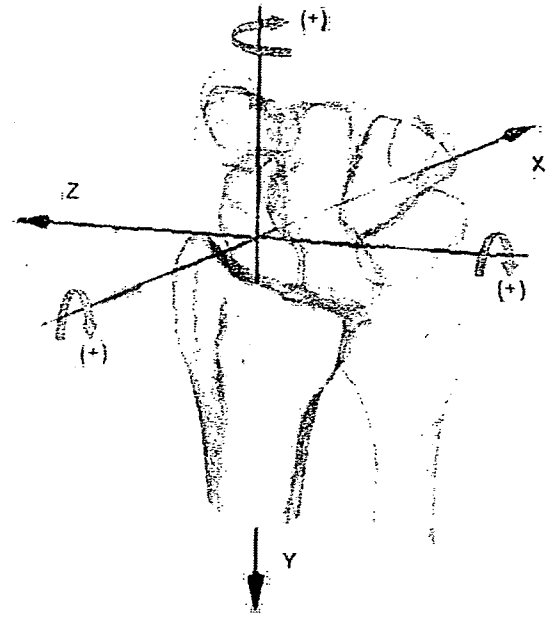

Fig. 2

A three-dimensional model showing details of the orthogonal reference system established in the radius as advocated by Belsole et al.[15] The Y axis was the longitudinal radial axis and indicated the proximal (+)/distal (-) direction; the Z axis was the line through the styloid perpendicular to the Y axis and indicated radial (+)/ulnar (-) displacement; the X axis was the line perpendicular to the YZ plane and indicated palmar (+)/dorsal (-) displacement. Rotation around the Z axis produced flexion (+)/extension (-); that around the Y axis pronation (+)/supination (-) and that around the X axis indicated ulnar (+)/radial (-) deviation.

line perpendicular to the YZ plane and indicated palmar (+)/dorsal (-) displacement. Rotation around the Z axis produced flexion (+)/extension (-); that around the Y axis pronation (+)/supination (-) and that around the X axis indicated ulnar (+)/radial (-) deviation (Fig. 2). Thus, we calculated as a 3D vector the translocation of each carpal bone relative to the reference system determined for the radius.[13,15]

Next, using the anatomical feature as described by Belsole et al[14] the local co-ordinate system for the scaphoid, lunate, and capitate was established to characterise carpal direction (Fig. 3). The X axis of the scaphoid was defined as its principal axis, calculated as the line on which the moment of inertia was smallest and which ran through the centroid. The Z axis was defined as the line running through the dorsal ridge of the scaphoid in the plane perpendicular to the X axis and the Y axis was the line perpendicular to the XZ plane. The X axis of the lunate was defined as the line through the palmar and dorsal poles, the Y axis as the line through the centroid, perpendicular to the X axis and the Z axis as the line perpendicular to the XY plane. The Y axis of the capitate was defined as its principal axis[14] and the Z axis as the line through the dorsal joint ridge of the capitate-hamate joint perpendicular to the Y axis, rotated +90° around the Y axis. The X axis was the line perpendicular to the YZ plane. From these planes the 3D vector of a carpus relative to the radius was calculated with six degrees of freedom using the Euler angle[12] method. This quantified the direction and rotation of each carpal bone in the RA wrist relative to the radius and compared their positions with those of a normal wrist.

With regard to evaluating the translocation of location of the centroid, the variation in size of each carpal bone needed to be considered, and the translocation index was used for the purpose. It was calculated by dividing each of the three components of the vector of the centroids of the carpal bones by the square root of the cross-section of the radius at a plane perpendicular to its longitudinal axis and passing through Lister's tubercle[16] (Fig. 4).

The translocation index was as follows:

$$(Tx, Ty, Tz) = x/\sqrt{S},\ y/\sqrt{S},\ z\sqrt{S},$$

where x, y and z represent the vectors of the centroid of the carpal bone, relative to the origin of the reference of the

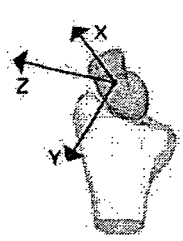

Fig. 3a

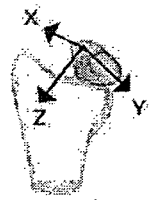

Fig. 3b

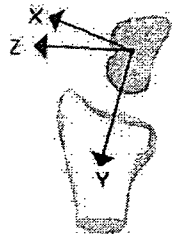

Fig. 3c

Diagram showing the orthogonal system as applied to a) the scaphoid, b) the lunate and c) the capitate according to Belsole et al.[14] The X axis of the scaphoid was defined as its principal axis, calculated as the line on which the moment of inertia was smallest and which ran through the centroid. The Z axis was defined as the line running through the dorsal ridge of the scaphoid in the plane perpendicular to the X axis, and the Y axis was the line perpendicular to the XZ plane. The X axis of the lunate was defined as the line through the palmar and dorsal poles, the Y axis as the line through the centroid, perpendicular to the X axis, and the Z axis as the line perpendicular to the XY plane. The Y axis of the capitate was defined as its principal axis and the Z axis as the line through the dorsal joint ridge of the capitate-hamate joint perpendicular to the Y axis, rotated +90° around the Y axis. The X axis was the line perpendicular to the YZ plane.

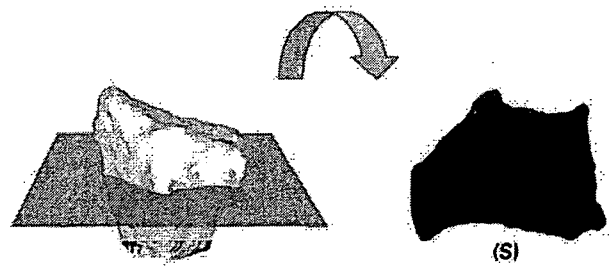

Fig. 4

Diagram showing the cross-section of the radius through Lister's tubercle, perpendicular to the longitudinal axis, S was the cross-sectional area of the radius (mm^2).

radius (mm) and S was the cross-sectional area of the radius (mm^2), at a plane perpendicular to its longitudinal axis at the level of Lister's tubercle (Fig. 4).

Statistical analysis. The left hand was converted to the orientation of the right and comparison of the results between the control and RA groups performed using standard statistical formulae based on the Mann-Whitney U-test. The results were deemed to be significant if $p \leq 0.05$.

Results

Centroid translocation. Three-dimensional images of the carpal bones showed that all centroids translocated not just in an ulnar direction, but also in the ulnar, proximal and volar direction, along the slope of the surface of the distal radius (Figs 5 and 6). Contacts between the radius and the scaphoid and the radius and the lunate were translocated ulnopalmarly and were incongruent in most cases. In the midcarpal joint, congruity was relatively well preserved compared with that of the radiocarpal joint in most cases (Fig. 7) while their radiographs showed joint narrowing (Fig. 1).

In the radioulnar deviation plane, the capitate ($p = 0.0011$) hamate, ($p = 0.0013$), lunate ($p < 0.0001$), scaphoid ($p = 0.0003$), triquetrum ($p < 0.0001$) and trapezoid ($p = 0.0197$), in RA wrists were significantly translocated to the ulnar side by a mean of 6.28, 4.68, 5.07, 7.10, 3.85 and 6.12 mm, respectively (Table I). In the flexion-extension plane all the centroids translocated in the palmar and proximal directions relative to the radius. The capitate ($p = 0.0083$), hamate ($p = 0.0037$) and scaphoid ($p = 0.0064$) in RA wrists were significantly translocated in the palmar direction by a mean of 3.21, 2.99 and 2.04 mm, respectively (Table I). The capitate ($p < 0.0001$), hamate ($p = 0.0037$), lunate ($p < 0.0001$), scaphoid ($p < 0.0001$) triquetrum ($p = 0.0011$), trapezium ($p < 0.0001$) and trapezoid ($p < 0.0001$) in RA wrists were significantly translocated proximally by a mean of 10.70, 9.41, 8.68, 6.90, 9.89, 11.37 and 13.30 mm, respectively (Table I).

Carpal rotation. The proximal row of RA wrists was flexed significantly compared with the normal wrists (Fig. 7b), the scaphoid at 25° ($p = 0.0003$) and the lunate at 10° ($p = 0.0311$) more than normal. In the pronation/supination plane, the scaphoid, lunate, and capitate did not supinate but were pronated 12°, 7° and 6°, respectively ($p = 0.053$, 0.147 and 0.356). The distal row was extended dorsally (Fig. 7c), as was the capitate by 12° ($p = 0.0387$) more than normal. The 3D images showed that the dorsally extended distal row corrected the hand to almost normal relative to the radius, by counteracting the flexion deformity of the proximal row.

Discussion

In the RA wrist, ligamentous laxity is probably the major cause of collapse and instability.[1] There are many reports which have attempted to measure the deformity radiologically,[2-4,6-8] but two-dimensional evaluation is of limited value. In our study, 3D imaging showed clearly that the rheumatoid carpus translocated obliquely in an ulnar, proximal and volar direction (Fig. 6). This quantitative technique allowed an easier understanding of this complex deformity. The direction of carpal translocation followed the natural slope of the joint surface of the distal radius which had a mean inclination of 24° in the coronal and 11° in the sagittal plane.[16,17] In normal wrists, displacement of the carpus was resisted mainly by the palmar and dorsal radiotriquetral and palmar radiolunate ligaments.[6,18,19] Their laxity probably allowed the 3D oblique translocation.

Rotational deformity, one of the most common deformities in RA, has been described qualitatively as carpal supination. Our 3D study, however, showed quantitatively that the main rotational deformity of the proximal row was

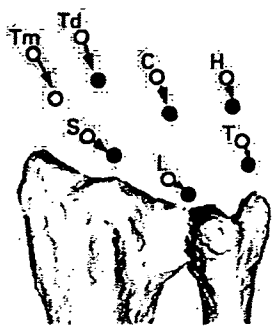

Fig. 5a

Fig. 5b

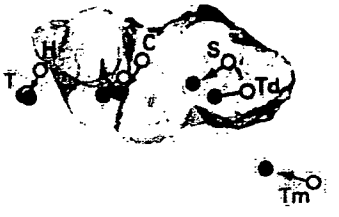

Fig. 5c

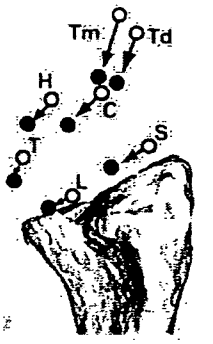

Fig. 5d

Diagrams showing centroid translocation (from a) a dorsal view, b) ulnar view, c) distal view and d) radiopalmar view. All the centroids translocated in an ulnar, proximal and volar direction. The trapezium translated slightly in a dorsal direction according to the X component but, overall, translocated in a palmar direction (Tm, trapezium; Td, trapezoid; C, capitate; H, hamate; S, scaphoid; L, lunate; and T, triquetrum).

Fig. 6a

Fig. 6b

Three-dimensional radiopalmar view of the translation of the carpus in a) a normal wrist and b) rheumatoid arthritis. The carpus translocates along the direction of the slope of the joint surface of the distal radius.

Fig. 7a

Fig. 7b

Fig. 7c

A three-dimensional view showing carpal rotation and joint congruity. Figure 7a – The normal wrist. Figure 7b – The radiocarpal joint is incongruent (arrow). Figure 7c – Joint congruity is relatively well-preserved in the midcarpal joint (arrowheads). In the sagittal plane, the scaphoid and lunate are flexed as in b) and the capitate is extended as in c).

palmar flexion with no significant rotation. Accurate estimation of carpal supination by plain radiography may not be easy since palmar subluxation of the distal radius in relation to the ulna makes it difficult to obtain a true lateral view for measurement of carpal rotation in the transverse plane.

We also noticed a different pattern of rotational deformity between the radiocarpal and midcarpal joints. Our 3D study showed that the proximal row as flexed at the radiocarpal joint and the distal row extended at the midcarpal joint (Fig. 7). While flexion of the proximal row was associated with translocation, the extension of the distal row was associated only with minor translocation. Although our patients had joint narrowing throughout the carpus, the congruity and function of the midcarpal joint were better preserved even in deformed RA wrists than at the radiocarpal joint.

Moritomo et al[20] proposed a self-stabilising mechanism which is stronger in the midcarpal than in the radiocarpal joint. A scaphoid under axial load against the trapezium tends to rotate in a flexion/ulnar direction. This turning effect is constrained by the extension/radial deviation moment of the triquetrum, leading to a stable equilibrium provided that the interosseous ligaments in the proximal row are intact. We speculated that, with loosening of many carpal ligaments, the radiocarpal joint may easily lose congruity. Whereas the deformity in this joint included translational and rotational elements, in the midcarpal joint the deformity was predominantly rotational. We considered the radiocarpal joint to be more incongruent and thereby more prone to cartilaginous damage.

Our study has limitations, the most important of which is that it was based on selected cases in which the whole carpal bones were shifted to the ulnar side, but the shapes were relatively recognisable on plain radiography. The other limitation was that age and gender were not fully matched between the RA and control wrists. It is possible that calculation of centroids and angles of rotation are influenced by erosion of the carpal bones with a subsequent alteration of shape. Our quantitative information,

Table I. *Details of translocation in the carpal bones*

	Centroid translocation																				
	Capitate			Hamate			Lunate			Scaphoid			Triquetrum			Trapezium			Trapezoid		
Direction	AD* (mm)	TI†	SD	AD (mm)	TI	SD	AD (mm)	TI	SD	AD (mm)	TI	SD	AD (mm)	TI	SD	AD (mm)	TI	SD	AD (mm)	TI	SD
Palmar																					
Normal	3.21	0.01	0.11	2.99	0.07	0.11	1.08	0.23	0.05	2.04	0.23	0.07	0.52	0.15	0.08	0.22	0.47	0.18	0.33	0.04	0.16
RA‡		0.17	0.16		0.22	0.21		0.33	0.18		0.37	0.16		0.20	0.21		0.54	0.16		0.07	0.17
Proximal																					
Normal	10.70	-0.57	0.14	9.41	-0.61	0.24	8.68	0.05	0.14	6.90	-0.20	0.06	9.89	-0.19	0.24	11.37	-0.83	0.16	13.30	-0.82	0.16
RA		-0.15	0.20		-0.26	0.20		0.48	0.27		0.10	0.15		0.25	0.27		-0.42	0.16		-0.32	0.17
Ulnar																					
Normal	6.28	0.19	0.19	4.68	0.70	0.19	5.07	0.35	0.09	7.10	-0.24	0.14	3.85	0.84	0.10	6.42	-0.49	0.26	6.12	-0.24	0.25
RA		0.52	0.18		1.04	0.23		0.66	0.14		0.05	0.14		1.17	0.16		-0.27	0.18		0.00	0.17

* AD, the absolute value of the difference of the mean translation (mm)
† TI, translocation index
‡ RA, rheumatoid arthritis

however, allowed early identification of the rheumatoid deformity and should be a guide to treatment, in particular in the decision as to whether to undertake radiocarpal fusion alone or to include the midcarpal joint.

Supplementary Material

A further opinion by Dr Klemens Trieb is available with the electronic version of this article on our website at www.jbjs.org.uk

No benefits in any form have been received or will be received from a commercial party related directly or indirectly to the subject of this article.

References

1. **Shapiro JS.** The wrist in rheumatoid arthritis. *Hand Clin* 1996;12:477-98.
2. **Kushner DM, Braunstein EM, Buckwalter KA, Krohn K, White HA.** Carpal instability in rheumatoid arthritis. *Can Assoc Radiol J* 1993;44:291-5.
3. **Muramatsu K, Ihara K, Tanaka H, Kawai S.** Carpal instability in rheumatoid wrists. *Rheumatol Int* 2004;24:34-6.
4. **Shapiro JS.** A new factor in the etiology of the ulnar drift. *Clin Orthop* 1970;68:32-43.
5. **Taleisnik J.** Rheumatoid synovitis of the volar compartment of wrist joint: its radiological signs and its contribution to wrist and hand deformity. *J Hand Surg [Am]* 1979;4:526-35.
6. **Flury MP, Herren DB, Simmen BR.** Rheumatoid arthritis of the wrist: classification related to the natural course. *Clin Orthop* 1999;366:72-7.
7. **Van Vught RM, van Jaarsveld CH, Hofman DM, Helders PJ, Bijlsma JW.** Patterns of disease progression in the rheumatoid wrist: a long-term follow-up. *J Rheumatol* 1999;26:1467-73.
8. **Shapiro JS.** Wrist involvement in rheumatoid arthritis swan-neck deformity. *J Hand Surg [Am]* 1982;7:484-91.
9. **Youm Y, McMurtry RY, Platt AE.** Kinematics of the wrist: an experimental study of radial-ulnar deviation and flexion-extension. *J Bone Joint Surg [Am]* 1978;60-A:423-31.
10. **Ochi T, Iwase R, Kimura T, et al.** Effect of early synovectomy on the course of rheumatoid arthritis. *J Rheumatol* 1991;18:1794-8.
11. **Lorensen WE, Cline HE.** Marching cubes: a high resolution 3D surface construction algorithm. *Computer Graphics* 1987;21:163-9.
12. **Goto A, Moritomo H, Murase T, et al.** In vivo three-dimensional wrist motion analysis using magnetic resonance imaging and volume-based registration. *J Orthop Res* 2005;23:750-6.
13. **Oka K, Moritomo H, Murase T, et al.** Patterns of carpal deformity in scaphoid nonunion: a 3-dimensional and quantitative analysis. *J Hand Surg [Am]* 2005;30:1136-44.
14. **Belsole RJ, Hilbelink DR, Llewellyn JA, et al.** Mathematical analysis of computed carpal models. *J Orthop Res* 1988;6:116-22.
15. **Belsole RJ, Bilbelink DR, Llewellyn JA, Dale M, Ogden JA.** Carpal orientation from computed reference axes. *J Hand Surg [Am]* 1991;16:82-90.
16. **Palmer AK.** Fractures of the distal radius. In: Green DP, ed. *Operative hand surgery.* Vol. 1. Third ed. New York: Churchill Livingstone, 1993:929-73.
17. **Schuind FA, Linscheid RL, An KN, Chao EY.** A normal data base of posteroanterior roentgenographic measurements of the wrist. *J Bone Joint Surg [Am]* 1992;74-A:1418-29.
18. **Cooney WP, Garcia-Elias M, Dobyns JH.** Anatomy of mechanics of carpal instability. *Surg Rounds Orthop* 1989;3:15-24.
19. **Mizuseki T, Ikuta Y.** The dorsal carpal ligament: their anatomy and function. *J Hand Surg [Br]* 1989;14:91-8.
20. **Moritomo H, Murase T, Goto A, et al.** In vivo three-dimensional kinematics of the midcarpal joint of the wrist. *J Bone Joint Surg [Am]* 2006;88-A:611-21.

DNA RESEARCH 13, 169–183 (2006) doi:10.1093/dnares/dsl006

Isolation and Expression Profiling of Genes Upregulated in Bone Marrow-Derived Mononuclear Cells of Rheumatoid Arthritis Patients

Nobuo NAKAMURA,[1,†] Yasunori SHIMAOKA,[2,†] Takahiro TOUGAN,[3] Hiroaki ONDA,[3,4] Daisuke OKUZAKI,[3] Hanjun ZHAO,[3] Azumi FUJIMORI,[3] Norikazu YABUTA,[3] Ippei NAGAMORI,[3] Akie TANIGAWA,[4] Jun SATO,[3] Takenori ODA,[5] Kenji HAYASHIDA,[6] Ryuji SUZUKI,[7] Masao YUKIOKA,[2] Hiroshi NOJIMA,[3,4,*] and Takahiro OCHI[7]

Center of Arthroplasty, Kyowakai Hospital, Suita, Japan[1], Yukioka Hospital, Osaka, Japan[2], Department of Molecular Genetics, Research Institute for Microbial Diseases, Osaka University, 3-1 Yamadaoka, Suita, Osaka 562-0031, Japan[3], Innovation Plaza Osaka, Izumi, Japan[4], Department of Rheumatology, NHO Osaka-Minami Medical Center, Kawachinagano, Japan[5], Hoshigaoka Kosei-Nenkin Hospital, Hirakata, Japan[6] and Clinical Research Center for Allergy and Rheumatology, National Sagamihara Hospital, 18-1 Sakura-dai, Sagamihara, Kanagawa 228-8522, Japan[7]

(Received 25 July 2006; revised 21 August 2006)

Abstract

We have comprehensively identified the genes whose expressions are augmented in bone marrow-derived mononuclear cells (BMMC) from patients with Rheumatoid Arthritis (RA) as compared with BMMCs from Osteoarthritis (OA) patients, and named them *AURA* after *au*gmented in *RA*. Both stepwise subtractive hybridization and microarray analyses were used to identify *AURA* genes, which were confirmed by northern blot analysis and/or reverse transcription polymerase chain reaction (RT–PCR). We also assessed their expression levels in individual patients by quantitative real-time RT–PCR. Of 103 *AURA* genes we have identified, the mRNA levels of the following 10 genes, which are somehow related to immune responses, were increased in many of the RA patients: *AREG* (=*AURA9*), FK506-binding protein 5 (FKBP5 = *AURA45*), C-type lectin superfamily member 9 (*CLECSF9* = *AURA24*), tyrosylprotein sulfotransferase 1 (*TPST1* = *AURA52*), lymphocyte G0/G1 switch gene (*G0S2* = *AURA8*), chemokine receptor 4 (CXCR4 = *AURA86*), nuclear factor-kappa B (NF-κB = *AURA25*) and two genes of unknown function (FLJ11106 = *AURA1*, BC022398 = *AURA2* and XM_058513 = *AURA17*). Since *AREG* was most significantly increased in many of the RA patients, we subjected it to further analysis and found that AREG-epidermal growth factor receptor signaling is highly activated in synovial cells isolated from RA patients, but not in OA synoviocytes. We propose that the expression profiling of these *AURA* genes may improve our understanding of the pathogenesis of RA.

Key words: stepwise subtraction; microarray; RA; OA; amphiregulin; synoviolin

1. Introduction

Rheumatoid arthritis (RA) is a systemic autoimmune disease characterized by arthritis that predominantly results in chronic inflammation of systemic joints associated with the overgrowth of synovial cells. This induces progressive cartilage and bone destruction in the joint and subsequent disability. Since RA pathogenesis is likely to involve genetic elements, a number of groups have subjected samples from healthy and affected individuals to DNA microarray analyses for a broad-scale comparison. These studies have provided

Communicated by Mitsuo Oshimura

* To whom correspondence should be addressed. Tel. +81-6-6875-3980, Fax. +81-6-6875-5192, E-mail: snj-0212@biken.osaka-u.ac.jp

† These authors contributed equally to this work.